Water-Soluble Pd_6L_3 Molecular Bowl for Separation of Phenanthrene from a Mixture of Isomeric Aromatic Hydrocarbons

Dharmraj Prajapati, Pallab Bhandari, Neal Hickey, and Partha Sarathi Mukherjee*

ABSTRACT: Phenanthrene is a high-value raw material in chemical industries. Separation of phenanthrene from isomeric anthracene continues to be a big challenge in the industry due to their very similar physical properties. Herein, we report the self-assembly of a water-soluble molecular bowl (**TB**) from a phenothiazine-based unsymmetrical terapyridyl ligand (**L**) and a *cis*-blocked 90° Pd(II) acceptor. **TB** featured an unusual bowl-like topology, with a wide rim diameter and a hydrophobic inner cavity fenced by the aromatic rings of the ligand. The above-mentioned features of **TB** allow it to bind polyaromatic hydrocarbons in its confined cavity. **TB** shows a higher affinity for phenanthrene over its isomer anthracene in water, which enables it to separate phenanthrene with ~93% purity from an equimolar mixture of phenanthrene and anthracene. **TB** is also able to extract pyrene with around ~90% purity from an equimolar mixture of coronene, perylene, and pyrene. Moreover, **TB** can be reused for several cycles without significant degradation in its performance as an extracting agent. This clean strategy of separation of phenanthrene and pyrene from a mixture of hydrophobic hydrocarbons by aqueous extraction is noteworthy.

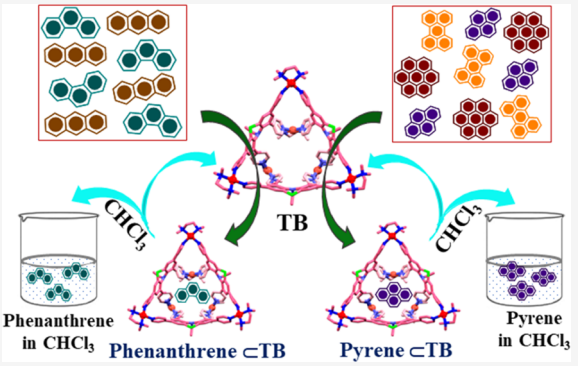

1. INTRODUCTION

Polycyclic aromatic hydrocarbons (PAHs) are environmental pollutants of concern on a global scale. PAHs are generally formed by incomplete combustion during the anthropogenic process of carbon-containing materials, such as fossil fuels, refuse, meat, wood, and tobacco.[1] PAHs are resistant to degradation, and uncontrolled exposure can cause several adverse effects on human health.[2] PAHs are insoluble or poorly soluble in water, and both their solubility in water and their volatility decrease with an increase in molecular weight.[3] In spite of this poor aqueous solubility and toxicity, PAHs are useful chemicals in the industrial chemistry processes for making medicines, dyes, plastics, pesticides, insecticides, and wood preservatives. They are also used for fabricating optical and electrical devices, which exploit their extended conjugation and planar structural features.[4] For example, pyrene and its derivatives are commercially important for making dyes and materials in light harvesting applications owing to their specific structural and electronic properties.[5] The usefulness of phenanthrene and pyrene is highly dependent on their purity. This has inspired the research community to develop efficient methods for the selective extraction of these PAHs. Solid-phase extraction and liquid−liquid extraction are commonly used techniques for the extraction of a wide variety of PAHs.[6] However, these conventional techniques suffer from many drawbacks, such as time-consuming multiple steps, poor reproducibility, and the requirement for large amounts of samples.[7,8] Inspired by natural host−guest systems, a wide variety of artificial hosts have been proposed as efficient alternatives to the classical extraction and purification techniques to overcome the above-mentioned drawbacks.[6d,9−11] Among the potential artificial hosts for separation applications, self-assembled discrete molecular architectures have gained special attention due to their easy accessibility in quantitative yields.[4,12−18] In fact, continuous efforts have been made to synthesize self-assembled coordination architectures for guest encapsulation,[12] catalysis,[13] sensing,[14] light harvesting,[15] stabilization of reactive species,[16] drug delivery,[17] and separation.[4,18] Separation of target molecules using water-soluble hosts is of enormous interest both from an industrial and an environmental point-of-view because they offer the possibility of a simple separation technique at ambient conditions.[4,10b,19] Coordination-driven self-assembly involving metals is an efficient method for designing such water-soluble hosts. Symmetrical ligands have been widely used for such coordination-driven self-assembly due to their selective confluence toward discrete assemblies. However, unsymmetrical ligands remain largely ignored due to the possibility

Scheme 1. Schematic Presentation of the Synthesis of L

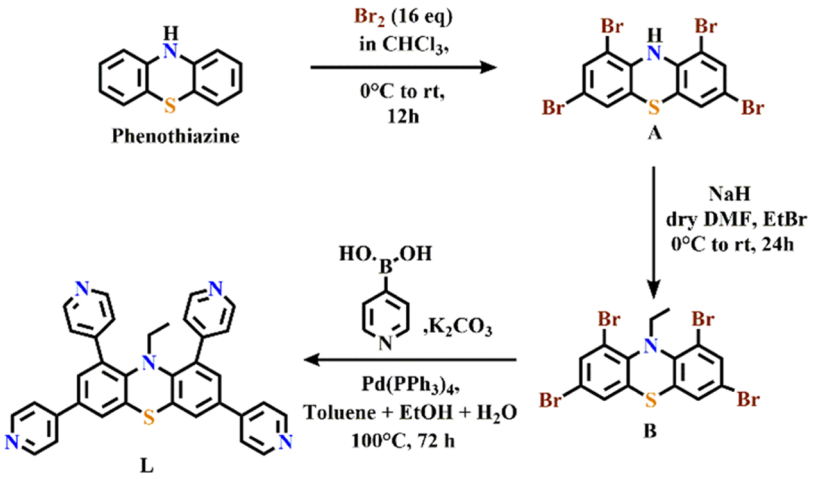

of the formation of multiple isomers upon binding of unsymmetrical donors around the metal centers.[20,21]

Herein, we report a water-soluble M_6L_3 molecular bowl (**TB**) which was obtained by the coordination-driven self-assembly of a new unsymmetrical phenothiazine-based tetrapyridyl donor **L** (Scheme 1) with a *cis*-blocked Pd(II) acceptor (Scheme 2). Due to the presence of two different pairs of donating 4-pyridyl moieties, the ligand **L** can bind in more than one fashion to potentially yield several structures. Despite these possibilities, a single discrete molecular bowl was formed. The bowl has a hydrophobic inner cavity defined by the aromatic backbone of **L** and a wide rim opening. This newly designed water-soluble architecture was found to be suitable for the encapsulation of PAHs in aqueous medium. Host–guest complexation and guest extraction studies with mixtures of PAHs revealed the formation of 1:1 host–guest complexes in all of the cases. **TB** can separate phenanthrene with ~93% purity by simple aqueous extraction from an equimolar mixture of isomeric anthracene and phenanthrene. Additionally, **TB** showed the ability to extract pyrene with ~90% purity from an equimolar mixture of coronene, perylene, and pyrene. Thus, **TB** represents a unique example of a water-soluble discrete architecture with an experimentally confirmed ability both for the challenging separation of hydrophobic phenanthrene from an isomeric mixture of anthracene and phenanthrene and for extraction of industrially important pyrene from a mixture of PAHs by a simple aqueous extraction technique.

Scheme 2. Self-assembly of a Pd_6L_3 Molecular Bowl (TB) and Its Preferential Host–guest Complexation with Phenanthrene and Pyrene

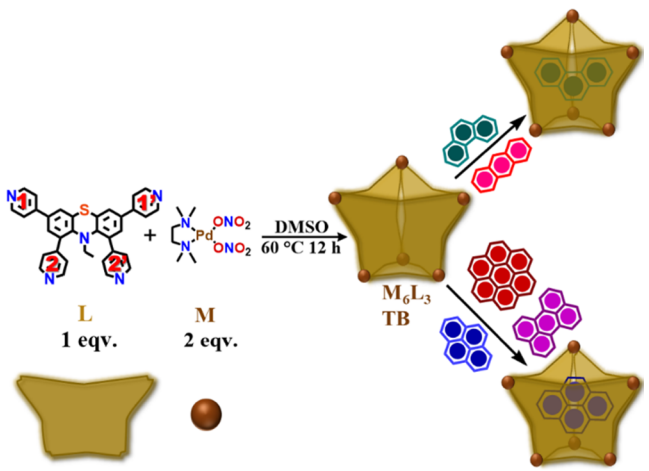

2. RESULTS AND DISCUSSION

2.1. Synthesis and Characterization. A new phenothiazine-based tetrapyridyl ligand 10-ethyl-1,3,7,9-tetra(pyridin-4-yl)-10H-phenothiazine (**L**) was synthesized by a Suzuki cross-coupling reaction of 1,3,7,9-tetrabromo-10-ethyl-10H-phenothiazine with pyridine-4-boronic acid under reflux conditions in a 5:5:1 (volume ratio) mixture of ethanol, toluene, and water (Scheme 1). **L** and its precursors were thoroughly characterized by multinuclear NMR, COSY, NOESY, and electrospray ionization-high-resolution mass spectrometry (ESI-HRMS) analyses (Figures S3–S9). For the self-assembly reaction, a mixture of **L** and *cis*-[(tmeda)Pd(NO_3)$_2$] (**M**) [tmeda = *N*,*N*,*N*′*N*′-tetramethylethane-1,2-diamine] in a 1:2 molar ratio was heated overnight in dimethyl sulfoxide (DMSO) at 60 °C with stirring. After completion of the reaction, the mixture turned into a clear yellow solution which, on treatment with an excess of ethyl acetate, yielded a yellow precipitate. The precipitate was thoroughly washed with acetone and diethyl ether, followed by overnight drying under vacuum to get the molecular bowl (**TB**). The ^{1}H NMR spectrum of **TB** (recorded in D_2O) exhibited that the methyl and methylene protons are in their expected positions (Figures S7 and S10) and ten distinct sharp peaks in the aromatic region, while the ^{1}H NMR spectrum of **L** showed only six peaks in the aromatic region. On the other hand, a single horizontal band in the diffusion-ordered NMR (^{1}H-DOSY, D_2O) of the product revealed the formation of a single self-assembled architecture (Figures 1 and S13).

Therefore, the presence of four extra peaks in the ^{1}H NMR spectrum of **TB** compared to ligand **L** indicates that the four distinct pairs of protons across the two different types of donating pyridyl moieties (marked as e, f, g, and h for **L** in Figure 1) are split into eight chemically distinct protons upon binding of **L** with the acceptor. Two different sets of peaks (e, e′, g, g′, and f, f′, h, h′) due to pyridyl moieties were assigned with the help of the ^{1}H–^{1}H COSY NMR study (Figure S11). This pattern advocated a differentiation of the protons due to

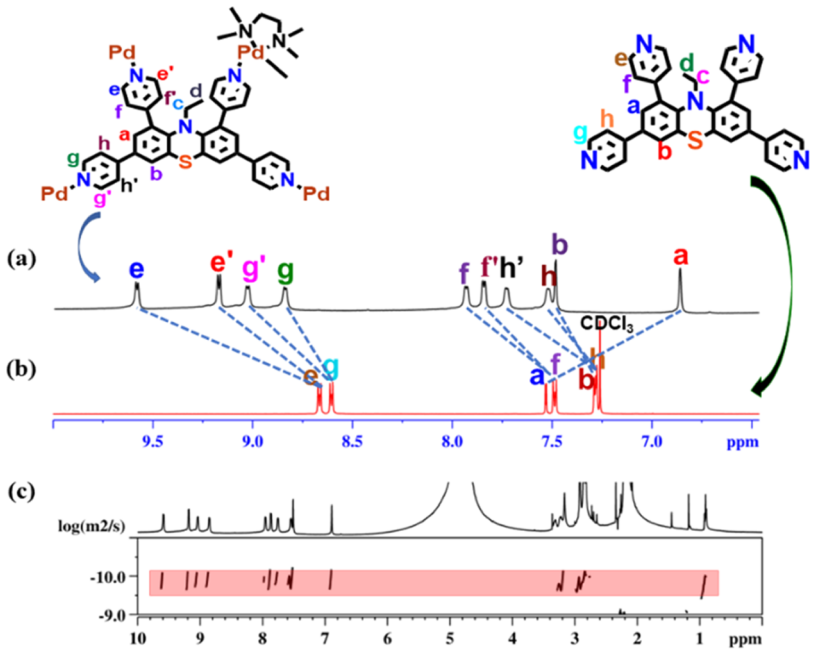

Figure 1. Stacked partial ^{1}H NMR spectra of (a) **TB** in D_2O, (b) ligand **L** in $CDCl_3$, and (c) diffusion-ordered ^{1}H NMR of **TB** in D_2O.

the locked orientations of the pyridyl moieties around the metal centers. Finally, a 2D ^{1}H−^{1}H NOESY NMR (Figure S12) study helped to assign all of the ^{1}H NMR peaks of the bowl.

To investigate the composition of **TB** in more detail, the water-soluble NO_3^- analogue of **TB** was converted into its PF_6^- analogue by adding an excess amount of KPF_6 to an aqueous solution of **TB**. The resulting precipitate was isolated and redissolved in acetonitrile for the ESI-HRMS study. Multiple prominent peaks were observed in the ESI-spectrum of **TB** at m/z = 1388.1335, 1004.8486, 774.8952, and 621.5807 that correspond to the charged fragments $[M_6L_3(NO_3)(PF_6)_8]^{3+}$, $[M_6L_3(NO_3)(PF_6)_7]^{4+}$, $[M_6L_3(NO_3)(PF_6)_6]^{5+}$, and $[M_6L_3(NO_3)(PF_6)_5]^{6+}$, respectively (Figures 2 and S14). The experimental isotopic distribution patterns of the peaks corresponding to the charged fragments matched well with the theoretically calculated isotopic distribution patterns (Figure S15), which unambiguously confirmed an M_6L_3 composition for the self-assembled **TB**.

Finally, to get further structural insight, suitable single crystals of **TB** were grown by diffusion of 1,4-dioxane vapor into an aqueous solution of the complex for X-ray diffraction (XRD). The single-crystal XRD study unambiguously confirmed the formation of an unusual M_6L_3 triangular molecular bowl (Figure 3). The crystallographic asymmetric unit (ASU) contains one donor **L** and two Pd(II) (**M**) acceptors (Figure 3a). As indicated above and in Figure 3a, **L** contains two pairs of nonidentical pyridyl units (1/1′ and 2/2′) and one of each of these pairs is coordinated to a Pd(II) center (1−Pd1 and 2−Pd2) in the ASU. However, two other crystallographically equivalent M_2L subunits are generated from this M_2L by 3_1 and 3_2 rotations around a 3-fold crystallographic axis parallel to the *c*-axis. This completes the bowl-like structure of **TB** with an M_6L_3 stoichiometry. The rotation relationship between the M_2L subunits means that each pair of pyridyl units is coordinated to a crystallographically equivalent Pd center (1 and 1′ to Pd1, 2, 2′ to Pd2). As all equivalent atoms generated by symmetry lie on

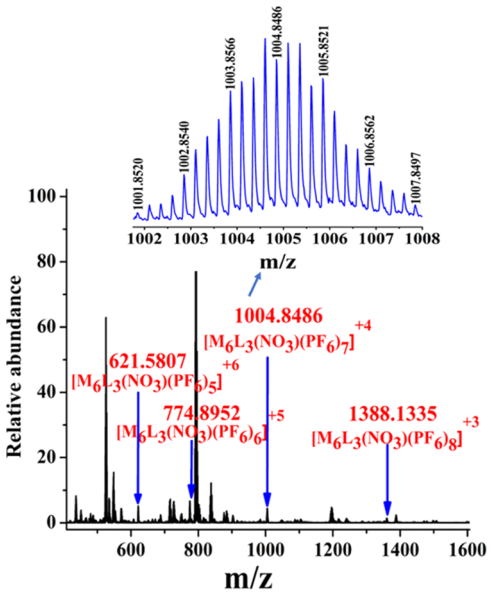

Figure 2. ESI-MS spectrum of the PF_6^- analogue of **TB** in acetonitrile. (Inset) The experimental isotopic distribution pattern of the $[M_6L_3(NO_3)(PF_6)_7]^{4+}$ fragment.

parallel planes, the plane of the Pd2 atoms defines the bottom of the bowl, while the plane of the Pd1 atoms defines its opening. A three-fold axis passes through its center.

The shape of the bowl may be described as an inverted truncated triangular pyramid, whose dimensions and faces are defined by the Pd1 and Pd2 atoms (Figures 3 and S1). Thus, the co-planar Pd2 atoms form an equilateral triangle base with a Pd2−Pd2 distance of 7.57 Å, while the open rim of the bowl is defined by Pd1 atoms, which also forms an equilateral triangle having a Pd1−Pd1 distance of 18.06 Å (Figures 3b and S1). The Pd1−Pd2 distances which define the edges of the bowl are 12.01 Å (Figures 3a and S1). The bowl faces are therefore delimited by Pd1 and Pd2 atoms, which form an isosceles trapezium of dimensions 7.57 Å × 18.06 Å × 12.01 Å

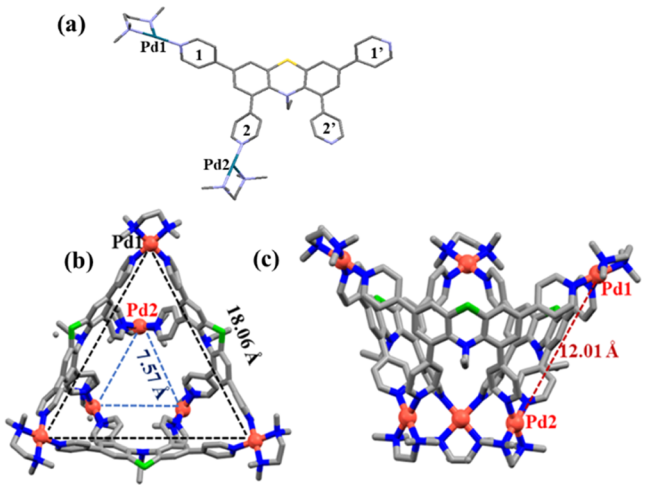

Figure 3. (a) Binding mode of **L** to two different Pd-centers. (b) Top view and (c) side view of the single-crystal structure of **TB** showing Pd−Pd distances. Color codes: gray = carbon, blue = nitrogen, green = sulfur, and red = palladium. Hydrogen atoms are omitted for better clarity.

(Figure S1). However, **L** has significantly curved away from the mean trapezium face defined by the 4 Pd atoms (Figure 3b), with out-of-plane distances of 2.248 and 2.756 Å to the phenothiazine N and S atoms, respectively. The internal dimensions of the bowl are, therefore, larger than those defined by the Pd atoms. Finally, the depth of the bowl, represented by the vertical height between the centroids of the Pd1 and Pd2 atoms (i.e., along the 3-fold axis), is 10.37 Å (Figure S1). It should also be noted that the bowl is not completely closed, as there are small openings along the edges and the bottom, which could allow passage of small molecules (Figure S2).

The geometry of the square planar Pd(II) centers is quite regular, with *cis* angles in the range of 84−95° for Pd1 and 87−93° for Pd2; and *trans* angles in the range of 178−180° for both Pd1 and Pd2 (Table S2). In fact, the steric strain necessary to close the structure appears to be mainly on the **L** ligands, which, as indicated above, are significantly curved. Unsurprisingly, the strain is bigger in the case of the pyridyl groups, which coordinate Pd2 at the base of the bowl and which are closer together (Table S3). Thus, with respect to the 6-atom mean planes of the coordinating pyridyl moieties, the Pd2 atom lies at out-of-plane distances of 0.488 and 0.325 Å for 2 and 2′. Similarly, the carbon atoms on the inner phenyl rings, which are directly bound to the pyridyl ring, lie at out-of-plane distances of 0.222 and 0.236 Å. In the case of Pd1, the corresponding out-of-plane distances are 0.556 and 0.463 Å for 1 and 1′, while they are almost co-planar for the ortho and the para-substituted C atoms, at only 0.067 and 0.001 Å.

Each type of Pd(II) center is coordinated to 6 N-donor atoms of **L**, which lie almost in the same plane; thus, for Pd1, the distance between the two parallel planes containing the 1 and 1′ N-donor atoms is 0.065 Å, while for Pd2 the distance between the parallel 2 and 2′ N-donor atom planes is 0.067 Å. Therefore, as also discussed above for the strain of **L**, while there are slight differences between each couple of pyridyl groups, all 6 pyridyl **L** units for each Pd(II) center are in very similar environments, giving rise to 2 sets of 6 pyridyl units in the structure (six for Pd1 and six for Pd2). Similarly, all of the tmeda N-donor atoms around each type of Pd(II) center lie almost in a plane, with distances between the symmetry-generated parallel planes of 0.068 Å for Pd1 and 0.086 for Pd. The crystal structure analysis reveals that each pyridyl moiety has four types of hydrogen atoms. The pyridyl moieties are locked in a conformation in which the ring is tilted with respect to the internal cavity, with one ortho- and one meta-carbon atom of the 4-pridyl ring tilted inward and the other two tilted outward with respect to the cavity (Figure 3).

Consequently, for each pyridyl, one type of hydrogen atom is oriented toward the cavity of **TB**, while the other is oriented outward. In this way, the equivalent protons of free **L** are split. The tilt of the mean planes of the pyridyl rings coordinated to each Pd is very similar (81.16 and 73.94° with respect to the Pd1 plane and 58.63 and 59.18° with respect to the Pd2 plane), so the signals for the corresponding proton should be very similar. Thus, the solid-state SC-XRD structure further accounts for the reason behind the splitting of the pyridyl protons in the ^{1}H NMR spectrum.

2.2. Guest Encapsulation Studies. As discussed above, characterization in both the solution and solid state revealed a bowl-shaped structure of **TB**. Many self-assembled architectures form closed structures, which inhibit the easy intake and release of large guest molecules. However, the current open molecular bowl should allow easy access to various guest molecules. Moreover, water-soluble **TB** has a hydrophobic pocket fenced by three ligands containing multiple aromatic rings (**L**). The water solubility, intrinsic hydrophobicity, and bowl-type structural features encouraged us to explore **TB** as a molecular host for the capture of various hydrophobic aromatic guest molecules in aqueous medium. For initial investigations, NBr (naphthalen-1-ylmethyl-2-bromo-2-methylpropanoate) was chosen as the aromatic guest. An excess amount of NBr was suspended in an aqueous solution of **TB** at room temperature. As expected, due to strong CH−π and π−π interactions of the NBr molecule with the aromatic wall of **TB**, the ^{1}H NMR spectrum resulted in a substantial downfield shift of the "e" proton (Figure 1) of the bowl from 9.59 to 9.68 ppm, along with the appearance of the guest (NBr) peaks in the upfield aromatic region (6.4−6.7 ppm) and a distinct methyl peak at 0.74 ppm for the propionate chain (Figures S16−S17). Further, a single horizontal band in the 2D DOSY NMR ($\log D = -9.76$) confirmed the formation of the host−guest adduct (Figure S19). 2D ^{1}H NOESY NMR for the adduct also exhibited cross-peaks, which supported the host−guest interaction (Figure S18). The host−guest stoichiometry was found to be 1:1 from the ^{1}H NMR integration of the guest's aromatic protons with TB's methyl (marked as d) protons. The host−guest stoichiometry was also rechecked after extraction of the guest in $CDCl_3$ in the presence of an internal standard.

This guest capture property prompted us to explore the scope of guest binding for polyaromatic hydrocarbon molecules within the molecular bowl. The scope of guest inclusion was examined by treating a D_2O solution of **TB** with excess amounts of various solid forms of PAHs (Figure 5) like naphthalene, anthracene, phenanthrene, pyrene, perylene, and coronene at room temperature with stirring for 24 h. The resulting suspensions were centrifuged to remove the excess guests, and the resulting solutions were examined by 1D and 2D NMR and UV−vis spectroscopic techniques. In all cases, the resulting host−guest complexes showed broadening and shifting of both host and guest protons in ^{1}H NMR, which indicated the complexation of the guest with the host. However, in some cases, the excessive broadening prevented

us from identifying the host−guest stoichiometry through simple integration of the host and guest peaks. Guests were therefore extracted, and the amounts were calculated with the help of trimethoxy benzene as an internal standard in $CDCl_3$. Additionally, 2D DOSY NMR displayed single diffusion bands in all of the cases (Figures S28, S33, S38, S43, and S48).

In the case of naphthalene, the ^1H spectrum of the host−guest complex (naphthalene ⊂ **TB**) showed downfield shifting of the pyridyl protons with the appearance of an extra broad peak at 5.90 ppm due to the guest (Figures 4b and S20−S21).

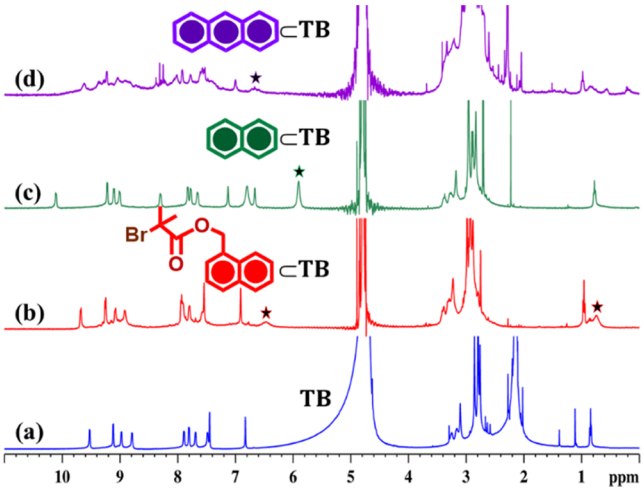

Figure 4. Partial ^1H NMR stack plot of (a) **TB**, (b) NBr ⊂ **TB**, (c) naphthalene ⊂ **TB**, and (d) anthracene ⊂ **TB** in D_2O showing the change in NMR upon guest encapsulation by **TB**. Star-marked peaks correspond to the encapsulated guests.

Such a downfield shift of the host's peaks and an upfield shift of the guest's peaks indicated strong hydrophobic interactions of the guest with the aromatic walls of **TB** (Figures S20−S21). 2D ^1H NOESY analysis revealed a cross peak between the naphthalene protons signal and the H_h and H_a proton signals of the host (Figure S23). Additionally, a single diffusion band ($\log D = -9.85$) for all of the signals corresponding to the host−guest complex in 2D DOSY NMR confirmed the encapsulation of the guest (Figure S22). The host−guest stoichiometry was estimated to be 1:1 by comparing the integration of the guest's broad peak (5.90 ppm) to the integration of the methyl H_d peak of the host (0.77 ppm) in the ^1H NMR spectrum of the naphthalene ⊂ **TB** complex. The host−guest ratio was further verified by extracting the guest from the aqueous solution of the naphthalene ⊂ **TB** complex in $CDCl_3$ in the presence of trimethoxy benzene as an internal standard (Figure S24). In a similar way, the host−guest complexation for other PAHs (Figure 5) was studied by ^1H NMR (Figures S25−S49). The broadening of the host peaks in the ^1H NMR spectra of other PAHs ⊂ **TB** was assumed to be due to the motion of the guest molecules inside the host cavity. Therefore, the stoichiometry was determined (1:1) by the guest extraction strategy in the $CDCl_3$ solvent as employed in the case of naphthalene.

Host−guest complexation was further explored by the UV−visible study. The UV−vis spectra of donor **L** and **TB** were recorded in $CHCl_3$ and H_2O, respectively (Figures S50−S51). The spectrum of **L** contains three absorption bands at 247, 269, and 307 nm, which are due to the $\pi-\pi^*$ transition, and a broad signal centered at around 456 nm, which could be

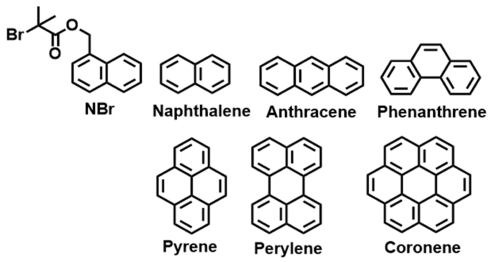

Figure 5. Guests used for the host−guest complexation with the host **TB**.

attributed to the $n-\pi^*$ transition (Figures S50). **TB** showed a strong absorption band at 203 nm, along with three broad bands around 257, 291, and 372 nm, which are due to the $\pi-\pi^*$ transition from the ligand units (Figures 6 and S51). The phenanthrene uptake resulted in a ≈7 nm red shift of the broad band at 257 nm, along with the appearance of a narrow absorption band at 250 nm due to the phenanthrene $\pi-\pi^*$ transition (Figure 6a). Similarly, for anthracene ⊂ **TB**, the peak corresponding to **TB** was red-shifted (257−260 nm) upon complexation with anthracene. Moreover, two new broad shoulders in the range of 240−255 nm and three broad peaks in the range of 345−410 were found in anthracene ⊂ **TB** (Figure 6a), which are in good agreement with the characteristic absorption of anthracene in MeOH/water.[4b,22] Pyrene ⊂ **TB** resulted in a ≈5 nm red shift of the broad band at 257 nm, along with the appearance of two broad shoulders at around 272 nm and 334 nm due to pyrene. In the case of perylene ⊂ **TB**, the peak due to **TB** was red-shifted (257 to 259 nm) upon encapsulation. The appearance of three new broad humps in the range of 390−460 nm indicated encapsulation of perylene (Figure 6b). A red shift (≈3 nm) of the broad band at 257 nm for corornene ⊂ **TB** was also observed, along with an absorption band at 290 nm and two broad bands at around 293 and 360 nm due to coronene. This absorption profile of corornene ⊂ **TB** is in good agreement with the characteristic absorption of coronene. Similarly, naphthalene ⊂ **TB** and NBr ⊂ **TB** show characteristic absorption bands at 219 and 222 nm (Figure S51), which are in good agreement with the literature reports on ethanol/water for naphthalene.[23]

TB is, therefore, a potential host for various PAHs in aqueous medium. The guest uptake affinity of **TB** toward PAHs was quantified in terms of binding constants (K_a) from the UV−visible titration experiments. As PAHs are insoluble in water, UV−visible titration was performed in a mixture of solvents (H_2O/MeOH). An aqueous solution of **TB** (10^{-5} M) was titrated with the methanol solution of the guests (10^{-3} M) at 25 °C (Figures S52−S55). From the titration experiments, the change in absorbance at 372 nm [ΔA_{372} (nm)] for phenanthrene, naphthalene, and NBr and the change in absorbance at 445 nm [ΔA_{445} (nm)] for pyrene were plotted against their respective equivalents. The titration data were fitted well with a 1:1 host−guest binding model. The binding constants were calculated to be ≈2.6×10^5 M^{-1} for phenanthrene and 5.3×10^4 M^{-1} for pyrene by fitting the titration data in Benesi−Hildebrand plots (B−H plots).[4b,24] We did a control experiment by adding methanol to the aqueous solution of **TB** to confirm the changes in absorbance are due to the guest binding by **TB**, not because of methanol addition (Figure S56). Unfortunately, binding constants for anthracene, perylene, and coronene could not be calculated

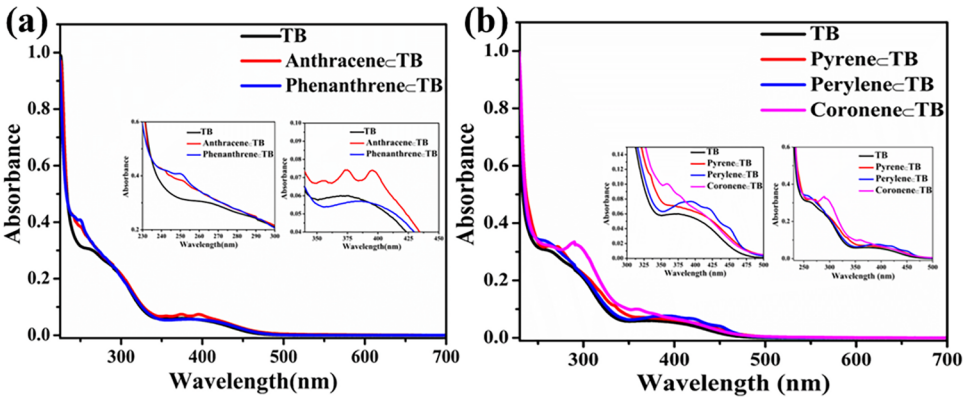

Figure 6. Normalized absorption spectra of (a) **TB**, phenanthrene ⊂ **TB**, anthracene ⊂ **TB**, (b) **TB**, pyrene ⊂ **TB**, perylene ⊂ **TB**, and coronene ⊂ **TB** at room temperature in water (10^{-5} M solution). Inset pictures show enlarged absorption spectra.

due to immediate saturation upon addition of small amounts of guests during titrations. However, a competitive guest uptake experiment was carried out with **TB** in the presence of an equimolar mixture (3 equiv of each guest with respect to **TB**) of solid anthracene, phenanthrene, pyrene, perylene, and coronene, which clearly revealed that **TB** has the highest uptake of phenanthrene and the lowest uptake of perylene. Analysis of the ^{1}H NMR spectrum (Figure S57) of the solution obtained by extraction with $CDCl_3$ of the encapsulated host–guest adducts in the D_2O supernatant indicated binding uptakes for the PAHs by **TB** of ~60, 33.5, 5.1, 0.94, and 0.65% for phenanthrene, pyrene, anthracene, coronene, and perylene, respectively. The relatively high selectivity of **TB** for the structurally similar guests, phenanthrene and pyrene, was presumably due to the more compatible fitting of those guests within the inner hydrophobic cavity of **TB**.

The host–guest structures, with the guests (naphthalene, phenanthrene, and pyrene), which were found to exhibit a strong binding constant, were investigated computationally using a gas phase semiempirical method in the ground state. The optimized structure for pyrene ⊂ **TB** displayed an energy-minimized structure where the pyrene guest was aligned perpendicularly to the host's walls inside the cavity (Figure S58). Similarly, naphthalene and phenanthrene were found to be perpendicularly aligned inside the hydrophobic cavity of the host **TB** in the optimized energy-minimized structure (Figure S59). DFT studies suggested that the efficient encapsulations were favored by the multiple CH···π interactions between the guest's protons with the aromatic backbones of the host. Thus, encapsulation of larger guests like perylene and coronene is disfavored due to size mismatching.

2.3. Separation of Phenanthrene from Anthracene. The binding affinity of **TB** for phenanthrene is higher than that of anthracene because of better size compatibility. This interesting observation led us to explore the bowl **TB** as a separating agent for phenanthrene from isomeric mixtures of phenanthrene and anthracene (Scheme 3). To check this, first, we investigated the competitive binding of phenanthrene and anthracene with the host **TB** in aqueous medium. A yellow D_2O solution of the host–guest complex of phenanthrene was treated with 3 equiv of solid anthracene and stirred for 24 h at room temperature (**TB** = 5.4×10^{-3} M). After the removal of the unbound guests, the clear D_2O solution gave almost unchanged ^{1}H NMR. Next, we did an experiment in a reverse manner, 3 equiv of solid phenanthrene were added to the D_2O solution of anthracene ⊂ **TB** and stirred for 24 h at room

Scheme 3. Schematic Presentation of Separation of Phenanthrene from a Mixture of Anthracene and Phenanthrene or Separation of Pyrene from a Mixture of Perylene, Coronene, and Pyrene by TB

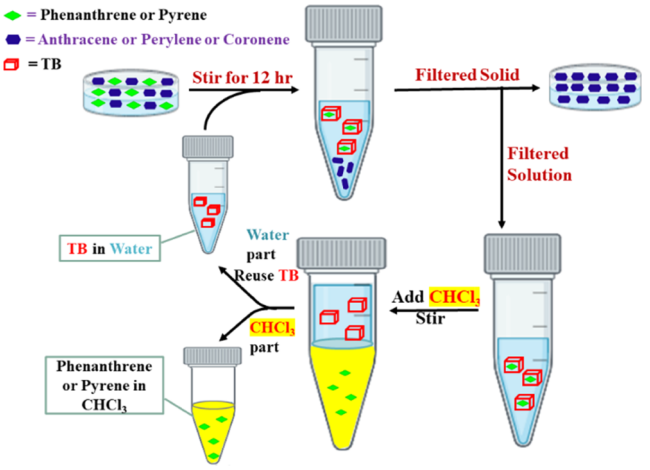

temperature (**TB** = 5.4×10^{-3} M). The centrifuged D_2O solution showed an NMR pattern like that of phenanthrene ⊂ **TB**. Thus, the treatment of phenanthrene with the anthracene ⊂ **TB** solution replaced the bound anthracene, while the reverse process was not successful. To check the efficiency of **TB** for the separation of phenanthrene from anthracene, an equimolar mixture of solid phenanthrene and anthracene was added to a D_2O solution of **TB** and stirred for 24 h at room temperature. The ^{1}H NMR of the supernatant was identical to that of phenanthrene ⊂ **TB**. Furthermore, to verify the above result, the sequestered guest was extracted with chloroform. The extracted chloroform solution was evaporated, and the isolated solid was redissolved in $CDCl_3$ for ^{1}H NMR analysis (Figure 7d and S60). ^{1}H NMR revealed 93% phenanthrene content in the mixture (Figure 7d). Thus, the **TB** bowl is a potential host for the separation of phenanthrene from isomeric anthracene with 93% purity by simple aqueous extraction.

2.4. Selective Guest Encapsulation: Pyrene vs Other PAHs. Based on the stronger binding ability of **TB** for pyrene, we further investigated the potential of **TB** as an extracting agent for industrially important pyrene from a mixture of pyrene, perylene, and coronene. To test this, excess amounts of solid pyrene, perylene, and coronene (5 equiv of each) were

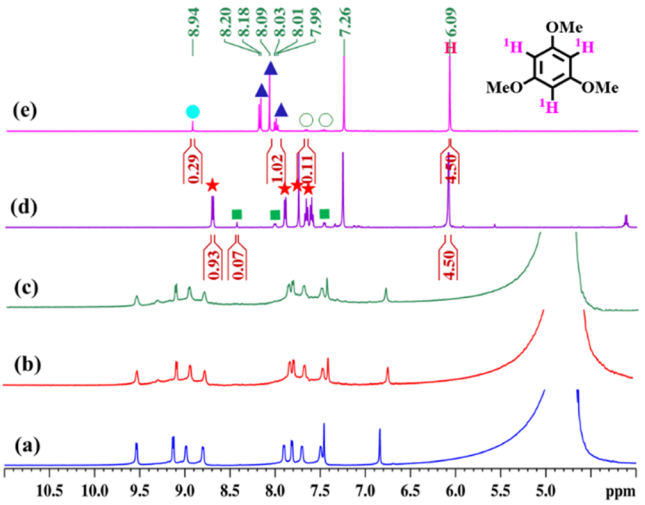

Figure 7. Partial ^{1}H NMR spectra of **TB** (a), **TB** recovered after 5 cycles of use for phenanthrene separation (b), **TB** recovered after (5 cycles of) pyrene separation (c), the $CDCl_3$ extract of the aqueous solution formed by treating an equimolar mixture of phenanthrene and anthracene with **TB** (d), and the $CDCl_3$ extract of the aqueous solution formed by treating an equimolar mixture of pyrene, perylene, and coronene with **TB** (e). Peaks from phenanthrene, anthracene, pyrene, coronene, and perylene are shown by the star, square, triangle, sphere, and empty circle, respectively. The peak for trimethoxy benzene (internal standard) is shown by H.

added to a D_2O solution of **TB** (**TB** = 5.4×10^{-3} M) and stirred for 24 h at room temperature. The yellow suspension was then centrifuged to remove the excess guests, and the clear supernatant was examined by ^{1}H NMR. The resultant ^{1}H NMR spectrum was much like that of pyrene ⊂ **TB**, but the peaks were broad in nature. Hence, for further verification, the guests were extracted in chloroform and analyzed by ^{1}H NMR. The ^{1}H NMR spectrum of the isolated solid gave signals corresponding to 90.8% pyrene, 4.3% coronene, and 4.9% perylene (Figures 7e and S62). Therefore, the **TB** bowl could also be used for the extraction of pyrene from mixtures of pyrene, perylene, and coronene with good purity.

The reusability of the bowl **TB** was tested for separation experiments. After extraction, the D_2O solution of the host **TB** exhibited an almost identical ^{1}H NMR spectrum to that of the as-synthesized bowl (Figures 7b,c, S61, and S63). Additionally, ESI-MS analysis confirmed the presence of the intact host **TB** (Figure S64). This prompted us to reuse the molecular bowl for phenanthrene and pyrene isolation. For this, the extracted **TB** solution was reused for five cycles for phenanthrene separation. It was found that it can separate phenanthrene without any significant reduction in efficiency (Figure S60). The same reusability was found when it was tested for pyrene extraction (Figure S62).

3. CONCLUSIONS

In conclusion, a unique molecular bowl (**TB**) with a wide open rim has been synthesized by the metal–ligand coordination-driven self-assembly of a 90° Pd(II) acceptor (**M**) with a new phenothiazine-based unsymmetrical tetrapyridyl ligand **L** in a 6:3 stoichiometry. Despite the possibility of the formation of multiple conformational isomers due to different binding modes of the unsymmetric ligand **L**, a single self-assembled molecular bowl formed exclusively. In an aqueous solution, the molecular bowl **TB** was able to bind a series of PAHs (naphthalene, anthracene, phenanthrene, pyrene, perylene, and coronene) of different sizes, which are otherwise insoluble in water in the absence of **TB**. Moreover, the specific structural features of **TB** and its hydrophobic cavity made it an efficient host for the selective capture of phenanthrene and pyrene. NMR and UV–vis studies indicated the formation of 1:1 host–guest complexes with different PAHs. UV–visible titration and competitive guest binding experiments revealed stronger binding of the host with phenanthrene and pyrene over other tested PAHs. This stronger uptake affinity of **TB** toward phenanthrene was employed for the separation of phenanthrene with 93% purity from an equimolar mixture of isomeric phenanthrene and anthracene by simple aqueous extraction. This is an important finding, as the separation of these two isomers is challenging in industry due to their similar physical properties. Moreover, **TB** was utilized for the extraction of industrially important pyrene with a ∼90% purity from the mixture of pyrene, perylene, and coronene. Importantly, the host **TB** was reused for five cycles without any significant loss in the efficiency of separation. Thus, the current studies may engender new designs and synthetic strategies for constructing a series of dissymmetrical supramolecular hosts by tuning the symmetry of building blocks. The newly engineered hosts containing specific nanocavities could be applied for selective separations and extractions of various industrially important organic guest molecules. Moreover, we believe that our present report shows a simple way of separating phenanthrene from its isomer anthracene and the extraction of pyrene from a solid mixture of PAHs in water.

■ ASSOCIATED CONTENT

Supporting Information

The Supporting Information is available free of charge at https://pubs.acs.org/doi/10.1021/acs.inorgchem.3c01156.

Experimental section, multinuclear NMR (^{1}H, ^{13}C, DOSY, COSY, NOESY) spectra, mass spectra, DFT studied data, photophysical data, and CIF (CCDC No. 2239766) (PDF)

Accession Codes

CCDC 2239766 contains the supplementary crystallographic data for this paper. These data can be obtained free of charge via www.ccdc.cam.ac.uk/data_request/cif, or by emailing data_request@ccdc.cam.ac.uk, or by contacting The Cambridge Crystallographic Data Centre, 12 Union Road, Cambridge CB2 1EZ, UK; fax: +44 1223 336033.

■ AUTHOR INFORMATION

Corresponding Author

Partha Sarathi Mukherjee − *Department of Inorganic and Physical Chemistry, Indian Institute of Science, Bangalore 560012, India;* orcid.org/0000-0001-6891-6697; Phone: 91-80-2293-3352; Email: psm@iisc.ac.in; Fax: 91-80-2360-1552

Authors

Dharmraj Prajapati − *Department of Inorganic and Physical Chemistry, Indian Institute of Science, Bangalore 560012, India*

Pallab Bhandari − *Department of Inorganic and Physical Chemistry, Indian Institute of Science, Bangalore 560012, India;* orcid.org/0000-0002-5990-9062

Neal Hickey − *Center of Excellence in Biocrystallography, Department of Chemical and Pharmaceuticals Sciences, University of Trieste, Trieste 34127, Italy;* orcid.org/0000-0003-1271-5719

Complete contact information is available at: https://pubs.acs.org/10.1021/acs.inorgchem.3c01156

Notes

The authors declare no competing financial interest.

■ ACKNOWLEDGMENTS

P.S.M. acknowledges the SERB (NEW DELHI) for financial support. The authors acknowledge the NMR facility at the IPC department (DST-FIST scheme).

■ REFERENCES

(1) (a) Cai, Y.; Yan, Z.-H.; Wang, N.-Y.; Cai, Q.-Y.; Yao, S.-Z. a. Preparation of naphthyl functionalized magnetic nanoparticles for extraction of polycyclic aromatic hydrocarbons from river waters. *RSC Adv.* **2015**, *5*, 56189−56197. (b) Sharma, P.; Bano, A.; Singh, S. P.; Sharma, S.; Xia, C.; Nadda, A. K.; Lam, S. S.; Tong, Y. W. Engineered microbes as effective tools for the remediation of polyaromatic aromatic hydrocarbons and heavy metals. *Chemosphere* **2022**, *306*, No. 135538. (c) Song, G.; Lu, C.; Lin, J.-M. Application of surfactants and microemulsions to the extraction of pyrene and phenanthrene from soil with three different extraction methods. *Anal. Chim. Acta* **2007**, *596*, 312−318. (d) Sushkova, S. N.; Vasilyeva, G. K.; Minkina, T. M.; Mandzhieva, S. S.; Tjurina, I. G.; Kolesnikov, S. I.; Kizilkaya, R.; Askin, T. New method for benzo[a]pyrene analysis in plant material using subcritical water extraction. *J. Geochem. Explor.* **2014**, *144*, 267−272. (e) Wang, J.; Odinga, E. S.; Zhang, W.; Zhou, X.; Yang, B.; Waigi, M. G.; Gao, Y. Polyaromatic hydrocarbons in biochars and human health risks of food crops grown in biochar-amended soils: A synthesis study. *Environ. Int.* **2019**, *130*, No. 104899. (f) Wicht, A.-J.; Heye, K.; Schmidt, A.; Oehlmann, J.; Huhn, C. The wastewater micropollutant carbamazepine in insectivorous birds—an exposure estimate. *Anal. Bioanal. Chem.* **2022**, *414*, 4909−4917.

(2) (a) Graham, M. C.; Allan, R.; Fallick, A. E.; Farmer, J. G. Investigation of extraction and clean-up procedures used in the quantification and stable isotopic characterisation of PAHs in contaminated urban soils. *Sci. Total Environ.* **2006**, *360*, 81−89. (b) Manousi, N.; Zachariadis, G. A. Recent Advances in the Extraction of Polycyclic Aromatic Hydrocarbons from Environmental Samples. *Molecules* **2020**, *25*, 2182. (c) Miège, C.; Dugay, J.; Hennion, M. C. Optimization, validation and comparison of various extraction techniques for the trace determination of polycyclic aromatic hydrocarbons in sewage sludges by liquid chromatography coupled to diode-array and fluorescence detection. *J. Chromatogr. A* **2003**, *995*, 87−97. (d) Pérez, R. A.; Albero, B.; Tadeo, J. L.; Fraile, M. V.; Sánchez-Brunete, C. Determination of PAHs in soil leachates by magnetic solid-phase extraction using nanoparticles and gas chromatography-tandem mass spectrometry. *Anal. Methods* **2014**, *6*, 1941−1950. (e) Yadav, V. K.; Malik, P.; Tirth, V.; Khan, S. H.; Yadav, K. K.; Islam, S.; Choudhary, N.; Inwati, G. K.; Arabi, A.; Kim, D. H.; Jeon, B. H. Health and Environmental Risks of Incense Smoke: Mechanistic Insights and Cumulative Evidence. *J. Inflammation Res.* **2022**, *15*, 2665−2693.

(3) Zhang, X.; Xie, S.; Paau, M. C.; Zheng, B.; Yuan, H.; Xiao, D.; Choi, M. M. F. Ultrahigh performance liquid chromatographic analysis and magnetic preconcentration of polycyclic aromatic hydrocarbons by Fe3O4-doped polymeric nanoparticles. *J. Chromatogr. A* **2012**, *1247*, 1−9.

(4) (a) Chakraborty, D.; Saha, R.; Clegg, J. K.; Mukherjee, P. S. Selective separation of planar and non-planar hydrocarbons using an aqueous Pd6 interlocked cage. *Chem. Sci.* **2022**, *13*, 11764−11771. (b) Liu, Y.; Wang, H.; Shangguan, L.; Liu, P.; Shi, B.; Hong, X.; Huang, F. Selective Separation of Phenanthrene from Aromatic Isomer Mixtures by a Water-Soluble Azobenzene-Based Macrocycle. *J. Am. Chem. Soc.* **2021**, *143*, 3081−3085. (c) Sainaba, A. B.; Venkateswarulu, M.; Bhandari, P.; Arachchige, K. S. A.; Clegg, J. K.; Mukherjee, P. S. An Adaptable Water-Soluble Molecular Boat for Selective Separation of Phenanthrene from Isomeric Anthracene. *J. Am. Chem. Soc.* **2022**, *144*, 7504−7513. (d) Zhang, D.; Ronson, T. K.; Lavendomme, R.; Nitschke, J. R. Selective Separation of Polyaromatic Hydrocarbons by Phase Transfer of Coordination Cages. *J. Am. Chem. Soc.* **2019**, *141*, 18949−18953.

(5) Canton-Vitoria, R.; Sayed-Ahmad-Baraza, Y.; Pelaez-Fernandez, M.; Arenal, R.; Bittencourt, C.; Ewels, C. P.; Tagmatarchis, N. Functionalization of MoS2 with 1,2-dithiolanes: toward donor-acceptor nanohybrids for energy conversion. *npj 2D Mater. Appl.* **2017**, *1*, No. 13.

(6) (a) Burel, A.; Brugman, S. J. T.; Mignot, M.; Cartigny, Y.; Tisse, S.; Couvrat, N.; Peulon-Agasse, V.; Cardinael, P.; Coquerel, G. Phenanthrene Purification: Comparison of Zone Melting and Co-Crystallization. *Chem. Eng. Technol.* **2016**, *39*, 1317−1325. (b) Couvrat, N.; Burel, A.; Tisse, S.; Cartigny, Y.; Coquerel, G. Combining zone melting and preparative chromatography to purify Phenanthrene. *J. Therm. Anal. Calorim.* **2013**, *112*, 293−300. (c) Goodarznia, I.; Esmaeilzadeh, F. Solubility of an Anthracene, Phenanthrene, and Carbazole Mixture in Supercritical Carbon Dioxide. *J. Chem. Eng. Data* **2002**, *47*, 333−338. (d) Kitt, J. P.; Harris, J. M. Confocal Raman Microscopy for in Situ Detection of Solid-Phase Extraction of Pyrene into Single C18−Silica Particles. *Anal. Chem.* **2014**, *86*, 1719−1725.

(7) (a) Filippou, O.; Bitas, D.; Samanidou, V. Green approaches in sample preparation of bioanalytical samples prior to chromatographic analysis. *J. Chromatogr. B* **2017**, *1043*, 44−62. (b) Nazario, C. E. D.; Fumes, B. H.; da Silva, M. R.; Lanças, F. M. New materials for sample preparation techniques in bioanalysis. *J. Chromatogr. B* **2017**, *1043*, 81−95. (c) Patejko, M.; Jacyna, J.; Markuszewski, M. J. Sample preparation procedures utilized in microbial metabolomics: An overview. *J. Chromatogr. B* **2017**, *1043*, 150−157.

(8) (a) Arthur, C. L.; Pawliszyn, J. Solid phase microextraction with thermal desorption using fused silica optical fibers. *Anal. Chem.* **1990**, *62*, 2145−2148. (b) Weems, H. B.; Mushtaq, M.; Fu, P. P.; Yang, S. K. Direct separation of non-K-region mono-ol and diol enantiomers of phenanthrene, benz[a]anthracene, and chrysene by high-performance liquid chromatography with chiral stationary phases. *J. Chromatogr. A* **1986**, *371*, 211−225. (c) Yang, Y.; Liu, M.; Wang, L.; Fu, J.; Yan, C.; Zhou, J. L. Sorption behavior of phenanthrene in Yangtze estuarine sediments: sequential separation. *Mar. Pollut. Bull.* **2011**, *62*, 1025−1031.

(9) (a) Li, N.; Jiang, H.-L.; Wang, X.; Wang, X.; Xu, G.; Zhang, B.; Wang, L.; Zhao, R.-S.; Lin, J.-M. Recent advances in graphene-based magnetic composites for magnetic solid-phase extraction. *TrAC, Trends Anal. Chem.* **2018**, *102*, 60−74. (b) Manousi, N.; Gomez-Gomez, B.; Madrid, Y.; Deliyanni, E. A.; Zachariadis, G. A. Determination of rare earth elements by inductively coupled plasma-mass spectrometry after dispersive solid phase extraction with novel oxidized graphene oxide and optimization with response surface methodology and central composite design. *Microchem. J.* **2020**, *152*, No. 104428. (c) Manousi, N.; Zachariadis, G. A.; Deliyanni, E. A.; Samanidou, V. F. Applications of Metal-Organic Frameworks in Food Sample Preparation. *Molecules* **2018**, *23*, 2896. (d) Riahi-Zanjani, B.; Balali-Mood, M.; Asoodeh, A.; Es'haghi, Z.; Ghorani-Azam, A. Developing a new sensitive solid-phase microextraction fiber based on carbon nanotubes for preconcentration of morphine. *Appl. Nanosci.* **2018**, *8*, 2047−2056.

(10) (a) Guo, C.; Sedgwick, A. C.; Hirao, T.; Sessler, J. L. Supramolecular fluorescent sensors: An historical overview and update. *Coord. Chem. Rev.* **2021**, *427*, No. 213560. (b) Jie, K.; Zhou, Y.; Li, E.; Huang, F. Nonporous Adaptive Crystals of Pillararenes. *Acc. Chem. Res.* **2018**, *51*, 2064−2072. (c) Kołodziejski, M.; Brock, A. J.; Kurpik, G.; Walczak, A.; Li, F.; Clegg, J. K.; Stefankiewicz, A. R. Charge Neutral [Cu2L2] and [Pd2L2] Metallocycles: Self-Assembly, Aggregation, and Catalysis. *Inorg. Chem.* **2021**, *60*, 9673−9679. (d) Wu, Y.; Zhou, J.; Li, E.; Wang,

M.; Jie, K.; Zhu, H.; Huang, F. Selective Separation of Methylfuran and Dimethylfuran by Nonporous Adaptive Crystals of Pillararenes. *J. Am. Chem. Soc.* **2020**, *142*, 19722−19730. (e) Zhou, Y.; Jie, K.; Zhao, R.; Li, E.; Huang, F. Highly Selective Removal of Trace Isomers by Nonporous Adaptive Pillararene Crystals for Chlorobutane Purification. *J. Am. Chem. Soc.* **2020**, *142*, 6957−6961.

(11) (a) Chakraborty, D.; Mukherjee, P. S. Recent trends in organic cage synthesis: push towards water-soluble organic cages. *Chem. Commun.* **2022**, *58*, 5558−5573. (b) Dey, A.; Chand, S.; Maity, B.; Bhatt, P. M.; Ghosh, M.; Cavallo, L.; Eddaoudi, M.; Khashab, N. M. Adsorptive Molecular Sieving of Styrene over Ethylbenzene by Trianglimine Crystals. *J. Am. Chem. Soc.* **2021**, *143*, 4090−4094. (c) Ding, Y.; Alimi, L. O.; Moosa, B.; Maaliki, C.; Jacquemin, J.; Huang, F.; Khashab, N. M. Selective adsorptive separation of cyclohexane over benzene using thienothiophene cages. *Chem. Sci.* **2021**, *12*, 5315−5318. (d) Hua, B.; Ding, Y.; Alimi, L. O.; Moosa, B.; Zhang, G.; Baslyman, W. S.; Sessler, J.; Khashab, N. M. Tuning the porosity of triangular supramolecular adsorbents for superior haloalkane isomer separations. *Chem. Sci.* **2021**, *12*, 12286−12291. (e) Zhang, G.; Ding, Y.; Hashem, A.; Fakim, A.; Khashab, N. M. Xylene isomer separations by intrinsically porous molecular materials. *Cell Rep. Phys. Sci.* **2021**, *2*, No. 100470.

(12) (a) Howlader, P.; Ahmed, S.; Mondal, S.; Zangrando, E.; Mukherjee, P. S. Conformation-Selective Self-Assembly of Pd6 Trifacial Molecular Barrels Using a Tetrapyridyl Ligand. *Inorg. Chem.* **2022**, *61*, 8121−8125. (b) Kaphan, D. M.; Levin, M. D.; Bergman, R. G.; Raymond, K. N.; Toste, F. D. A supramolecular microenvironment strategy for transition metal catalysis. *Science* **2015**, *350*, 1235−1238. (c) Meeuwissen, J.; Reek, J. N. H. Supramolecular catalysis beyond enzyme mimics. *Nat. Chem.* **2010**, *2*, 615−621. (d) Percástegui, E. G.; Ronson, T. K.; Nitschke, J. R. Design and Applications of Water-Soluble Coordination Cages. *Chem. Rev.* **2020**, *120*, 13480−13544. (e) Saha, R.; Sahoo, J.; Venkateswarulu, M.; De, M.; Mukherjee, P. S. Shifting the Triangle−Square Equilibrium of Self-Assembled Metallocycles by Guest Binding with Enhanced Photosensitization. *Inorg. Chem.* **2022**, *61*, 17289−17298.

(13) (a) Bar, A. K.; Chakrabarty, R.; Mukherjee, P. S. Self-Assembly of a Pd6−Molecular Double-Square and a Cu3-Trigonalbipyramidal Cage via a New Tripodal Flexible Ligand. *Inorg. Chem.* **2009**, *48*, 10880−10882. (b) Kaphan, D. M.; Toste, F. D.; Bergman, R. G.; Raymond, K. N. Enabling New Modes of Reactivity via Constrictive Binding in a Supramolecular-Assembly-Catalyzed Aza-Prins Cyclization. *J. Am. Chem. Soc.* **2015**, *137*, 9202−9205. (c) Martí-Centelles, V.; Lawrence, A. L.; Lusby, P. J. High Activity and Efficient Turnover by a Simple, Self-Assembled "Artificial Diels−Alderase". *J. Am. Chem. Soc.* **2018**, *140*, 2862−2868. (d) Roy, B.; Devaraj, A.; Saha, R.; Jharimune, S.; Chi, K.-W.; Mukherjee, P. S. Catalytic Intramolecular Cycloaddition Reactions by Using a Discrete Molecular Architecture. *Chem. - Eur. J* **2017**, *23*, 15704−15712. (e) Saha, R.; Mondal, B.; Mukherjee, P. S. Molecular Cavity for Catalysis and Formation of Metal Nanoparticles for Use in Catalysis. *Chem. Rev.* **2022**, *122*, 12244−12307. (f) Sinha, I.; Mukherjee, P. S. Chemical Transformations in Confined Space of Coordination Architectures. *Inorg. Chem.* **2018**, *57*, 4205−4221.

(14) (a) Purba, P. C.; Venkateswaralu, M.; Bhattacharyya, S.; Mukherjee, P. S. Silver(I)−Carbene Bond-Directed Rigidification-Induced Emissive Metallacage for Picric Acid Detection. *Inorg. Chem.* **2022**, *61*, 713−722. (b) Yan, X.; Wang, H.; Hauke, C. E.; Cook, T. R.; Wang, M.; Saha, M. L.; Zhou, Z.; Zhang, M.; Li, X.; Huang, F.; Stang, P. J. A Suite of Tetraphenylethylene-Based Discrete Organoplatinum(II) Metallacycles: Controllable Structure and Stoichiometry, Aggregation-Induced Emission, and Nitroaromatics Sensing. *J. Am. Chem. Soc.* **2015**, *137*, 15276−15286.

(15) (a) Acharyya, K.; Bhattacharyya, S.; Sepehrpour, H.; Chakraborty, S.; Lu, S.; Shi, B.; Li, X.; Mukherjee, P. S.; Stang, P. J. Self-Assembled Fluorescent Pt(II) Metallacycles as Artificial Light-Harvesting Systems. *J. Am. Chem. Soc.* **2019**, *141*, 14565−14569. (b) Ahmed, S.; Kumar, A.; Mukherjee, P. S. Tetraphenylethene-Based Emissive Pt(II) Coordination Polymer toward Artificial Light-Harvesting Systems with Sequential Energy Transfer. *Chem. Mater.* **2022**, *34*, 9656−9665. (c) Gorai, T.; Lovitt, J. I.; Umadevi, D.; McManus, G.; Gunnlaugsson, T. Hierarchical supramolecular co-assembly formation employing multi-component light-harvesting charge transfer interactions giving rise to long-wavelength emitting luminescent microspheres. *Chem. Sci.* **2022**, *13*, 7805−7813. (d) Hu, Y.-X.; Li, W.-J.; Jia, P.-P.; Wang, X.-Q.; Xu, L.; Yang, H.-B. Supramolecular Artificial Light-Harvesting Systems with Aggregation-Induced Emission. *Adv. Opt. Mater.* **2020**, *8*, No. 2000265. (e) Kumar, A.; Saha, R.; Mukherjee, P. S. Self-assembled metallasupramolecular cages towards light harvesting systems for oxidative cyclization. *Chem. Sci.* **2021**, *12*, 5319−5329.

(16) (a) Bhandari, P.; Modak, R.; Bhattacharyya, S.; Zangrando, E.; Mukherjee, P. S. Self-Assembly of Octanuclear PtII/PdII Coordination Barrels and Uncommon Structural Isomerization of a Photochromic Guest in Molecular Space. *JACS Au* **2021**, *1*, 2242−2248. (b) Grommet, A. B.; Lee, L. M.; Klajn, R. Molecular Photoswitching in Confined Spaces. *Acc. Chem. Res.* **2020**, *53*, 2600−2610. (c) Saha, R.; Mukherjee, P. S. Chemistry of photoswitching molecules in the confined nanospace of aqueous molecular vessels. *Dalton Trans.* **2020**, *49*, 1716−1720. (d) Yang, D.; Zhao, J.; Yu, L.; Lin, X.; Zhang, W.; Ma, H.; Gogoll, A.; Zhang, Z.; Wang, Y.; Yang, X.-J.; Wu, B. Air- and Light-Stable P4 and As4 within an Anion-Coordination-Based Tetrahedral Cage. *J. Am. Chem. Soc.* **2017**, *139*, 5946−5951. (e) Yanshyna, O.; Białek, M. J.; Chashchikhin, O. V.; Klajn, R. Encapsulation within a coordination cage modulates the reactivity of redox-active dyes. *Commun. Chem.* **2022**, *5*, No. 44.

(17) (a) Bhat, I. A.; Jain, R.; Siddiqui, M. M.; Saini, D. K.; Mukherjee, P. S. Water-Soluble Pd8L4 Self-Assembled Molecular Barrel as an Aqueous Carrier for Hydrophobic Curcumin. *Inorg. Chem.* **2017**, *56*, 5352−5360. (b) Lewis, J. E. M.; Gavey, E. L.; Cameron, S. A.; Crowley, J. D. Stimuli-responsive Pd2L4 metallosupramolecular cages: towards targeted cisplatin drug delivery. *Chem. Sci.* **2012**, *3*, 778−784. (c) Schmitt, F.; Freudenreich, J.; Barry, N. P.; Juillerat-Jeanneret, L.; Süss-Fink, G.; Therrien, B. Organometallic cages as vehicles for intracellular release of photosensitizers. *J. Am. Chem. Soc.* **2012**, *134*, 754−757. (d) Zhang, D.; Ronson, T. K.; Nitschke, J. R. Functional Capsules via Subcomponent Self-Assembly. *Acc. Chem. Res.* **2018**, *51*, 2423−2436.

(18) (a) Chang, X.; Lin, S.; Wang, G.; Shang, C.; Wang, Z.; Liu, K.; Fang, Y.; Stang, P. J. Self-Assembled Perylene Bisimide-Cored Trigonal Prism as an Electron-Deficient Host for C60 and C70 Driven by "Like Dissolves Like". *J. Am. Chem. Soc.* **2020**, *142*, 15950−15960. (b) Howlader, P.; Mondal, S.; Ahmed, S.; Mukherjee, P. S. Guest-Induced Enantioselective Self-Assembly of a Pd6 Homochiral Octahedral Cage with a C3-Symmetric Pyridyl Donor. *J. Am. Chem. Soc.* **2020**, *142*, 20968−20972. (c) Howlader, P.; Zangrando, E.; Mukherjee, P. S. Self-Assembly of Enantiopure Pd12 Tetrahedral Homochiral Nanocages with Tetrazole Linkers and Chiral Recognition. *J. Am. Chem. Soc.* **2020**, *142*, 9070−9078. (d) Nguyen, B.-N. T.; Thoburn, J. D.; Grommet, A. B.; Howe, D. J.; Ronson, T. K.; Ryan, H. P.; Bolliger, J. L.; Nitschke, J. R. Coordination Cages Selectively Transport Molecular Cargoes Across Liquid Membranes. *J. Am. Chem. Soc.* **2021**, *143*, 12175−12180. (e) Purba, P. C.; Maity, M.; Bhattacharyya, S.; Mukherjee, P. S. A Self-Assembled Palladium(II) Barrel for Binding of Fullerenes and Photosensitization Ability of the Fullerene-Encapsulated Barrel. *Angew. Chem., Int. Ed.* **2021**, *60*, 14109−14116. (f) Zhang, D.; Ronson, T. K.; Zou, Y.-Q.; Nitschke, J. R. Metal−organic cages for molecular separations. *Nat. Rev. Chem.* **2021**, *5*, 168−182. (g) Zhang, W.-Y.; Lin, Y.-J.; Han, Y.-F.; Jin, G.-X. Facile Separation of Regioisomeric Compounds by a Heteronuclear Organometallic Capsule. *J. Am. Chem. Soc.* **2016**, *138*, 10700−10707. (h) Zhu, C.; Tang, H.; Yang, K.; Fang, Y.; Wang, K.-Y.; Xiao, Z.; Wu, X.; Li, Y.; Powell, J. A.; Zhou, H.-C. Homochiral Dodecanuclear Lanthanide "Cage in Cage" for Enantioselective Separation. *J. Am. Chem. Soc.* **2021**, *143*, 12560−12566.

(19) (a) Martínez-Agramunt, V.; Eder, T.; Darmandeh, H.; Guisado-Barrios, G.; Peris, E. A Size-Flexible Organometallic Box for the Encapsulation of Fullerenes. *Angew. Chem., Int. Ed.* **2019**, *58*, 5682−

5686. (b) Ronson, T. K.; Meng, W.; Nitschke, J. R. Design Principles for the Optimization of Guest Binding in Aromatic-Paneled FeII4L6 Cages. *J. Am. Chem. Soc.* **2017**, *139*, 9698−9707. (c) Saura-Sanmartin, A.; Martinez-Cuezva, A.; Marin-Luna, M.; Bautista, D.; Berna, J. Effective Encapsulation of C60 by Metal−Organic Frameworks with Polyamide Macrocyclic Linkers. *Angew. Chem., Int. Ed.* **2021**, *60*, 10814−10819. (d) Szalóki, G.; Croué, V.; Carré, V.; Aubriet, F.; Alévêque, O.; Levillain, E.; Allain, M.; Aragó, J.; Ortí, E.; Goeb, S.; Sallé, M. Controlling the Host−Guest Interaction Mode through a Redox Stimulus. *Angew. Chem., Int. Ed.* **2017**, *56*, 16272−16276.

(20) Roy, B.; Ghosh, A. K.; Srivastava, S.; D'Silva, P.; Mukherjee, P. S. A Pd8 Tetrafacial Molecular Barrel as Carrier for Water Insoluble Fluorophore. *J. Am. Chem. Soc.* **2015**, *137*, 11916−11919.

(21) (a) Frank, M.; Krause, L.; Herbst-Irmer, R.; Stalke, D.; Clever, G. H. Narcissistic self-sorting vs. statistic ligand shuffling within a series of phenothiazine-based coordination cages. *Dalton trans.* **2014**, *43*, 4587−4592. (b) Frank, M.; Hey, J.; Balcioglu, I.; Chen, Y.-S.; Stalke, D.; Suenobu, T.; Fukuzumi, S.; Frauendorf, H.; Clever, G. H. Assembly and Stepwise Oxidation of Interpenetrated Coordination Cages Based on Phenothiazine. *Angew. Chem., Int. Ed.* **2013**, *52*, 10102−10106. (c) Frank, M.; Ahrens, J.; Bejenke, I.; Krick, M.; Schwarzer, D.; Clever, G. H. Light-Induced Charge Separation in Densely Packed Donor−Acceptor Coordination Cages. *J. Am. Chem. Soc.* **2016**, *138*, 8279−8287.

(22) Lima, A. L. C.; Farrington, J. W.; Reddy, C. M. Combustion-Derived Polycyclic Aromatic Hydrocarbons in the Environment—A Review. *Environ. Forensics* **2005**, *6*, 109−131.

(23) Chebbi, S.; Allouche, A.; Schwarz, M.; Rabhi, S. R. S.; Belkacemi, H.; Merabet, D. Treatment of produced water by induced air flotation: effect of both TWEEN 80 and ethanol concentrations on the recovery of PAHs. *Nova Biotechnol. Chim.* **2018**, *17*, 181−192.

(24) (a) Shi, Y.; Cai, K.; Xiao, H.; Liu, Z.; Zhou, J.; Shen, D.; Qiu, Y.; Guo, Q. H.; Stern, C.; Wasielewski, M. R.; Diederich, F.; Goddard, W. A., 3rd; Stoddart, J. F. Selective Extraction of C(70) by a Tetragonal Prismatic Porphyrin Cage. *J. Am. Chem. Soc.* **2018**, *140*, 13835−13842. (b) Thordarson, P. Determining association constants from titration experiments in supramolecular chemistry. *Chem. Soc. Rev.* **2011**, *40*, 1305−1323.